Moon-related nonthermal ions observed by Nozomi: Species, sources, and generation mechanisms

Yoshifumi Futaana and Shinobu Machida
Department of Geophysics, Kyoto University, Kyoto, Japan

Yoshifumi Saito, Ayako Matsuoka, and Hajime Hayakawa
Institute of Space and Astronautical Science, Sagamihara, Japan

Received 7 March 2002; revised 19 September 2002; accepted 9 October 2002; published 16 January 2003.

[1] The 3-D velocity distribution functions of nonthermal ions observed in the vicinity of the Moon have been analyzed to understand the interaction between the solar wind and the Moon. The observation was made during the lunar swing-by of the Nozomi spacecraft, and the closest approach was about 1.6 R_L from the Moon's surface. Both Nozomi and the Moon were located in the solar wind, and nonthermal ions were observed only when the spacecraft was very close to the Moon. The nonthermal ions were measured by a Particle Spectrum Analyzer/Ion Spectrum Analyzer (PSA/ISA) on board the Nozomi. After analyses and careful examination of the 3-D velocity distribution of the nonthermal ions, the characteristics of the nonthermal ions were revealed as follows: The nonthermal ions have a partial ring structure in the phase space, they are protons, their source location is the dayside of the Moon, and they have large velocities when they are generated. We propose the following scenario of a solar wind interaction with the Moon: The electromagnetic field in the vicinity of the Moon must have a dynamic structure, possibly a miniature bow shock associated with a local magnetic anomaly, where some of the solar wind protons are deflected violating their first adiabatic invariant. After the deflection, they move under the force of the convection electric field and gyrate around the magnetic field in the solar wind. This motion forms a partial ring structure with large initial velocities in the velocity phase space. *INDEX TERMS:* 2780 Magnetospheric Physics: Solar wind interactions with unmagnetized bodies; 2152 Interplanetary Physics: Pickup ions; 2164 Interplanetary Physics: Solar wind plasma; 6205 Planetology: Solar System Objects: Asteroids and meteoroids; 5421 Planetology: Solid Surface Planets: Interactions with particles and fields; *KEYWORDS:* nonthermal ions, partial ring structure, MHD shocks, lunar magnetic anomalies, miniature magnetosphere system, NOZOMI spacecraft

Citation: Futaana, Y., S. Machida, Y. Saito, A. Matsuoka, and H. Hayakawa, Moon-related nonthermal ions observed by Nozomi: Species, sources, and generation mechanisms, *J. Geophys. Res.*, *108*(A1), 1025, doi:10.1029/2002JA009366, 2003.

1. Introduction

[2] The interaction between the Moon and solar wind has been studied since the 1960s (see the review by *Schubert and Lichtenstein* [1974], and references therein).

[3] The first in situ observation of the lunar plasma environment was by the USSR Luna 2 and it revealed the absence of a noticeable lunar dipole magnetic field [*Dolginov et al.*, 1961].

[4] The basic nature of the interaction between the Moon and solar wind has been established by Explorer 35. Unlike the Earth, no global disturbances like bow shock have been detected by magnetic field observations [*Colburn et al.*, 1967; *Ness et al.*, 1967]. Measurements of the positive ion flux also support the absence of global disturbances in the vicinity of the Moon [*Lyon et al.*, 1967]. These results suggest that the Moon cannot disturb the solar wind plasma and the magnetic field in a steady state because the Moon has no global dipole magnetic field or a notable ionosphere.

[5] The Moon has small-scale magnetized regions called magnetic anomalies. Mapping of the lunar remanent magnetic field has been conducted since the Apollo program (e.g., see the review by *Dyal et al.* [1974], and references therein). *Lin et al.* [1988] reported that large magnetic anomalies are located at the antipodes of the four large young impact basins: Orientale, Imbrium, Serenitatis, and Crisium. Namely, large anomalies with horizontal scales of $\sim$1000 km are located on the lunar far-side. Recent magnetometer and electron reflectometer experiments on the Lunar Prospector globally mapped such lunar magnetic anomalies [*Lin et al.*, 1998; *Hood et al.*, 2001].

[6] Test particle calculations in the vicinity of the lunar magnetic anomalies were conducted by *Hood and Williams* [1989] and explained the correlation between the location of swirl-like high- and low-albedo marking of Reiner Gamma

0148-0227/03/2002JA009366$09.00

and the magnetic anomaly. They modeled the lunar magnetic anomaly by several buried dipoles. They ignored any collective effects of the plasma and any interaction with the interplanetary magnetic field in their calculations.

[7] Limb compressions, which are small-scale compressional disturbances of the magnetic field at or just in front of the lunar terminator, were observed by Apollo 15 and 16 and are statistically analyzed by *Russell and Lichtenstein* [1975]. *Russell and Lichtenstein* [1975] showed that the limb compressions appear only in specific selenographic regions and that the occurrence of the limb compressions is correlated with the magnetic field strength. They concluded the probable cause of limb compressions is the deflection of the solar wind by the lunar surface magnetic anomalies in the limb region.

[8] *Lin et al.* [1998] presented the observational evidence of the interaction between the lunar magnetic anomalies and the solar wind by a magnetometer on board Lunar Prospector. The observation showed that the increase in the magnetic field related to a magnetic anomaly disappeared when the solar wind dynamic pressure increased. They concluded that the observation of the increase in the magnetic field was due to the pile up of the interplanetary magnetic field.

[9] Two dimensional magnetohydrodynamic simulations were conducted by *Harnett and Winglee* [2000] that suggest formation of miniature magnetospheres. They concluded that the formation is realized when the field strength is above 10 nT at 100 km above the surface and when the solar wind ion density is below 40 cm^{-3}. They also suggested that the position and shape of the miniature bow shocks or magnetospheres are dramatically changed by the solar wind conditions.

[10] Measurements of nonthermal ions in the vicinity of the Moon in the solar wind have been observed by several satellites. The first reports about the escaped heavy ions originating from the Moon were by *Hilchenbach et al.* [1991, 1993]. They used a time-of-flight spectrometer SULEICA on the AMPTE/IRM satellite in the analysis and detected heavy ions with a mass range between 23 and 37 amu beyond the Earth's bow shock ($\sim$18.7 R_E from the Earth). They claimed that the likely sources on the Moon were a thin layer of lunar atmosphere or erosion processes on the lunar surface. *Mall et al.* [1998] statistically analyzed lunar-originated heavy ions by STICS on the WIND spacecraft. With its 17 lunar flybys which took place between 1995 and 1997, lunar originated ions were observed on the earthward side of the Moon as close as 17 lunar radii. The ion species were concluded to be O^+, Al^+, Si^+, and P^+. Test particle calculations of trajectories of the lunar originated heavy ions were reported by *Cladis et al.* [1994]. They pointed out that the phase space volume of the ions increases due to the diffusion and reflection by the Earth's bow shock and the deflection by the Earth's magnetosphere.

[11] The terrestrial bow shock produces nonthermal protons [*Asbridge et al.*, 1968]. In addition to the thermal solar wind protons, nonthermal protons with a partial shell structure or a partial ring structure, i.e, the nonthermal protons occupy partially filled shell or ring in the velocity space, have been observed. [e.g., *Paschmann et al.*, 1981; *Thomsen*, 1985]. Such ions are generated by a reflection of the solar wind protons due to the electric field at the shock surface.

Table 1. Basic Specifications of PSA/ISA

Energy Range	6 eV/q $\sim$ 16 keV/q
Energy Steps	32 steps
Energy Resolution	$\Delta E/E \sim 7.2\%$ (FWHM)
Field of View	4.4 deg $\times$ 180 deg
Angle Resolution	1.9 deg $\times$ 5.9 deg (FWHM) (maximum)
Time Resolution	3 dim. moment data/spin (maximum)
	3 dim. velocity distribution function/spin (maximum)
G-factor	8.84×10^{-5} cm^2 sr eV/eV at 22.5 deg $\times$ 4.4 deg

[12] Nonthermal ions, both proton and heavy ions like O^+, were also observed in the vicinity of comets [*Mukai et al.*, 1986; *Terasawa et al.*, 1986]. The velocity distribution function of the ions had a partial ring structure in the velocity space as a result of the $E \times B$-drift after neutral atoms or molecules of cometary origin are ionized. In the same way as comets, unmagnetized planets like Mars or Venus inject ions into the interplanetary space [*Lundin et al.*, 1989]. The ions are expected to exhibit a partial ring structure.

[13] This paper discuss nonthermal ions observed in the vicinity of the Moon. The observations were conducted with the Nozomi satellite during its lunar swing-by, and the closest approach was at an altitude of 2800 km. We show that the species of the nonthermal ions are proton and their generation is related to the Moon. Observations and analyses of lunar related nonthermal protons with 3-D velocity distributions have not been reported previously. We found that the nonthermal protons have a partial ring structure in the velocity space, which indicates that some dynamic electromagnetic structure, like miniature shocks, exist in the vicinity of the Moon and that they deflect the solar wind thermal ions.

2. Instrumentation

[14] The 3-D ion observations were performed using a Particle Spectrum Analyzer/Ion Spectrum Analyzer (PSA/ISA) mounted on the Nozomi spacecraft. The PSA/ISA is an electrostatic energy-per-charge analyzer for ions and can measure ions from 6 eV/q to 16 keV/q in 32 energy steps. With one spin rotation ($\sim$6.5 sec at the time of a lunar swing-by), the PSA/ISA can cover a full 4π steradian view angle with a 22.5° $\times$ 22.5° angular resolution. The basic specifications of the instrument are shown in Table 1.

[15] The time interval between each 3-D velocity distribution data is not regular due to the telemetry architecture. It is about 1 minute before 0736 UT, except for the data loss interval between 0718 and 0724 UT. Between 0742 and 0747 UT, it is every one spin time period, i.e., 6.5 sec, then it is 2 min after 0754 UT.

[16] The magnetic field was observed by using a magnetic field instrument (MPM/MGF), which is a three-axis fluxgate magnetometer installed at the end of a 5 m deployable mast [*Yamamoto and Tsuruda*, 1998]. However, we were unable to use MGF data for the period of the lunar swing-by, because the mast would not extend until the insertion of Nozomi into the Mars orbit. Therefore, the magnetic field data were contaminated by many kinds of electromagnetic noises of $\sim$1 nT originating from various instruments on board the Nozomi. The interplanetary magnetic field was

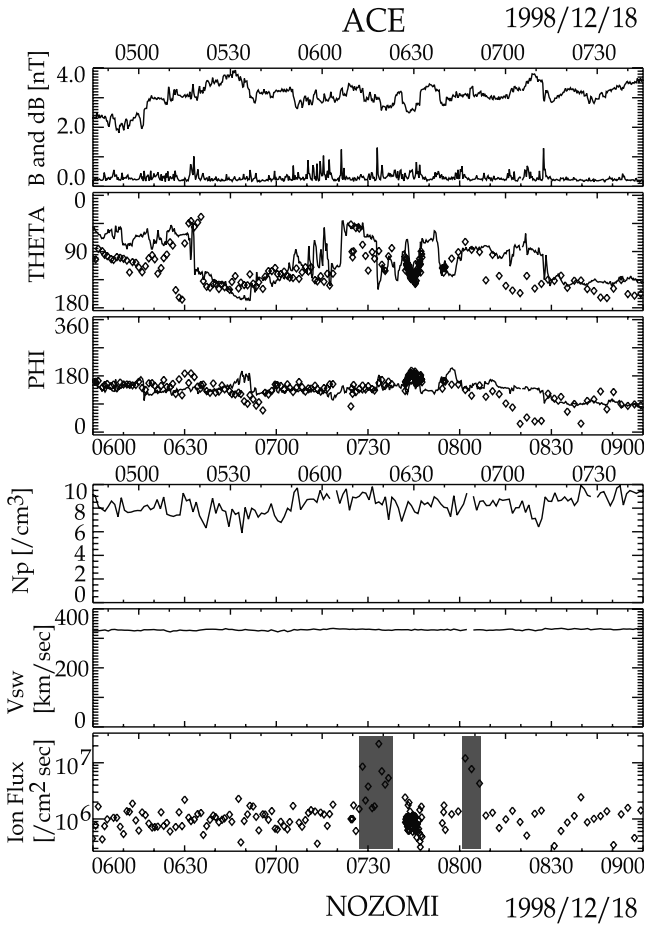

Figure 1. Time series of the magnetic field and the plasma moment data obtained by ACE and Nozomi. From top to bottom, the magnetic field strength and r.m.s., the ratio of those, the θ- and ϕ-components of the magnetic field directions, the solar wind velocity, and the nonsolar wind ion flux. The thin lines and the diamond marks in each panel are data obtained by ACE and Nozomi, respectively. Because Nozomi's magnetic field data are not available, the direction of the magnetic field was estimated by the electron velocity distribution. The time for ACE and Nozomi data was shown at the top and bottom of the plot. We assumed the solar wind propagation time to be 75 min from the magnetic field direction data.

about 3 nT during that interval, so relative errors in the magnetic field data were large. For these reasons, we did not use MPM/MGF data in this analysis.

[17] Instead, we estimated the magnetic field orientation from 3-D electron velocity distribution data. The 3-D electron data were obtained using the Particle Spectrum Analyzer/Electron Spectrum Analyzer (PSA/ESA), which can detect electrons with energies between 12 eV and 3 keV [*Machida et al.*, 1998]. We used temperature anisotropy of relatively high energy electrons (>100 eV), which tend to move along the magnetic field line and have a gyrotropic distribution, to determine the orientation of the magnetic field [*Futaana et al.*, 2001]. This estimation obviously has a 180° ambiguity. We checked ACE magnetic field data to determine the polarity of the estimated magnetic field orientation. The results are shown in the second and third panels of Figure 1, in which the θ- and ϕ-components of the IMF in the GSE coordinate system are shown. Solid lines show the ACE level 2 data and diamond symbols show our estimation. We shifted ACE data by 75 min to take account of the satellite locations. They indicate a very similar structure.

[18] Evaluation of the validity of the estimations should be clarified. One assumption of our estimation is that the velocity distributions of the solar wind electrons are gyrotropic. The solar wind electron component used in our analysis is called strahl, which has gyrotropic and field-aligned beam velocity distributions [*Montgomery et al.*, 1968; *Ogilvie et al.*, 1971; *Feldman et al.*, 1975]. If the beam width of the strahl is zero, our estimation is the least accurate due to the angular resolution of the PSA/ESA, which is 22.5°. The strahl component has a $30° \sim 40°$ beam width [see *Futaana et al.*, 2001, Plate 2]. In this case, the accuracy must be improved by more than 22.5° by a weighting effect of a multiangular observation.

[19] The accuracy of our estimation was also checked by comparing the estimated data with data of direct observations by MPM/MGF on other days when the contamination was small. We found that the standard deviation of our estimation was about 20°, which is comparable to the above value.

3. Observations

[20] (Figure 2a) shows locations of the Earth, the Moon, Nozomi, ACE, and the Earth's bow shock based on a model by *Peredo et al.* [1995] in the GSE coordinates on 18 December 1998. The direction of the magnetic field and the solar wind velocity is also indicated. Parameters used to derive the bow shock shape and location are the averaged value of the ACE observation.

[21] The trajectories of the Nozomi in the Lunar Centered GSE (LCGSE) coordinate system, which is centered on the Moon and has an orientation for each axis that is the same as in the GSE coordinate system, are shown in (Figure 2b). The Nozomi spacecraft approached the Moon at an altitude of approximately 2800 km at 0734 UT. Because it was a new moon on that day, the Moon was in the solar wind which almost flows along the *x axis*.

[22] Figure 3 shows a time series of the ion counts observed by PSA/ISA. From top to bottom, time series of the omnidirectional ion counts, solar wind thermal ion counts, and nonthermal ion counts are shown. A solar wind thermal component is a collimated beam that has a compact volume and has a clear boundary in the velocity phase space, so it is easy to separate a nonthermal component from a thermal one.

[23] The solar wind component has two peaks at velocities of ~350 km/sec and ~500 km/sec; one is for protons and the other is for alpha particles in (Figure 3b). The reason why the thermal component shows two peaks will be explained later.

[24] Nonthermal ions, in which we are interested, enhanced at around 0730 UT and past 0800 UT. They have the energies of ~1 keV which is as large as the solar wind ions. In the bottom panel of Figure 1, we show the time

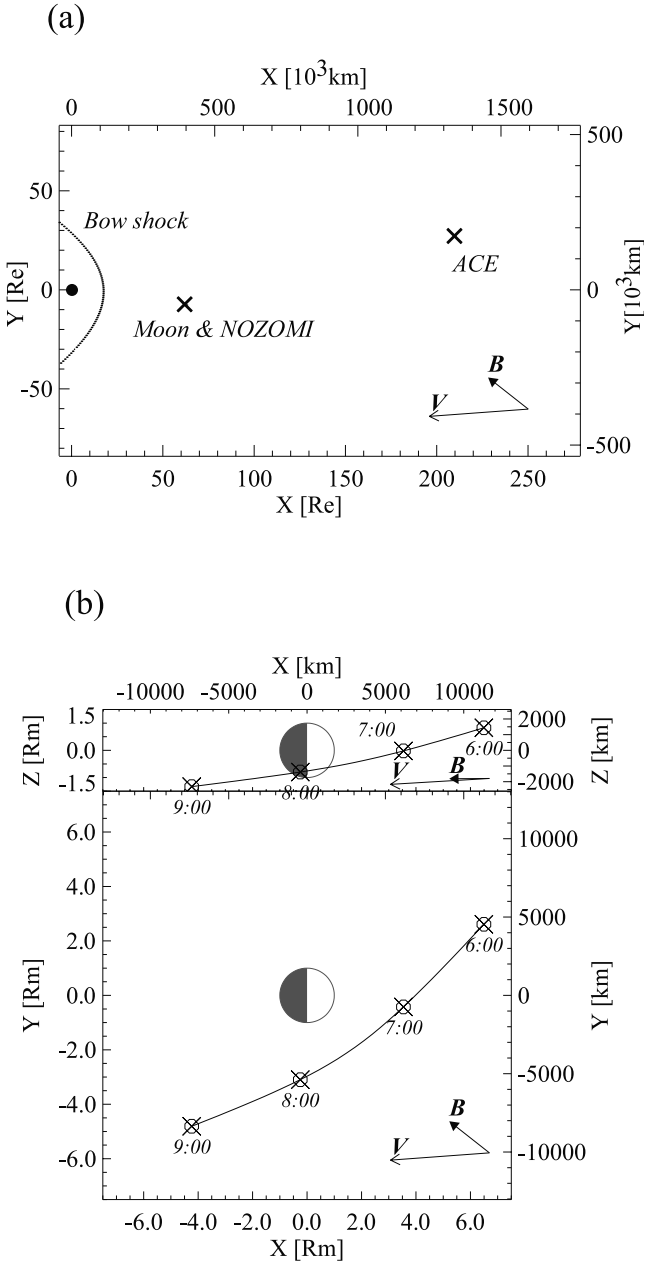

Figure 2. (a) Location of the Earth, the Moon, Nozomi, ACE, and the shape of the Earth's bow shock modeled by *Peredo et al.* [1995] in the GSE coordinate system. Directions of the averaged magnetic field and the solar wind velocity are also shown. (b) Trajectory of Nozomi during the lunar swing-by (0600–0900 UT) in the LCGSE coordinate system. The circle at the center of each panel represents the Moon. The curve in each panel shows the trajectory of Nozomi. The closest approach was at 0734 UT and the distance from the Moon center was ~2800 km.

series of the nonthermal ion flux observed by Nozomi in addition to the IMF data. The hatched intervals correspond to the time when the nonthermal ions appeared, and the Nozomi spacecraft was located very close to the Moon. Their flux is in the order of 10^6/cm^2 sec or 10^7/cm^2 sec, which is one or two orders of magnitude smaller than that of the solar wind.

[25] The relevant 3-D ion velocity distribution functions are shown in Figure 4. The top and bottom panels are for the same time interval for different view angles. The ions with velocities $V_x = -300$ to -500 km/sec are the solar wind ions, which are indicated by red frames. Remaining counts on (b), (c), and (e) are the nonthermal components.

[26] Because PSA/ISA is an energy-per-charge analyzer, we have no information on ion species. Throughout this paper, we based on the assumption that all ions are protons. This assumption is checked later and is confirmed to be valid.

[27] Figure 5 shows the velocity distribution projected onto a plane perpendicular to (a) the direction of the magnetic field and (b) the convection electric field. Here, V_B, V_E, and V_C represent the velocity parallel to the direction of the magnetic field, the convection electric field, and the $E \times B$-drift, respectively. Partial ring structures can be seen in (Figure 5a) and velocities parallel to the magnetic field are nearly constant in (Figure 5b).

[28] The formation mechanism of the partial ring structure is simple: the ions that have velocities different from solar wind ions start to gyrate around the magnetic field and drift toward the $E \times B$ direction with the convection electric field $E = -V_{SW} \times B$. Each ion has a circular trajectory in the $V_E - V_C$ space and the velocity parallel to the magnetic field is preserved. If we observe a limited portion of the ions, we can see a partial ring structure and a relatively constant velocity parallel to the magnetic field as shown in (Figures 5a and 5b).

4. Discussion

[29] One of the most important subjects of this study is the issue of the species, sources, and generation mechanisms of nonthermal ions. We discuss these subjects taking the plasma environment near the Moon into account.

4.1. Species of the Nonthermal Ions

[30] Because the PSA/ISA is an energy-per-charge analyzer, we do not have direct information on the mass and charge of the nonthermal ions. Analyzing the velocity distribution gives us information on the mass and charge of ions. The relationship between the observed and actual velocity of ions is as follows.

$$E_{obs} = E_{real}/q = \frac{m_p}{2}\frac{M}{q}v_{real}^2 = \frac{m_p}{2}v_{obs}^2, \quad (1)$$

so that

$$v_{obs} = \sqrt{\frac{M}{q}}v_{real}, \quad (2)$$

where m_p is the proton mass, M and q are the mass and charge of the observed ions normalized by those of the proton, E_{real} and v_{real} are the real energy and the real velocity of the observed ions, E_{obs} is the observed energy of the ions, and v_{obs} is the calculated velocity assuming that the observed ions are protons. If these ions are not protons, the observed velocities (v_{obs}) are $\sqrt{M/q}$ times larger than the real velocities (v_{real}).

[31] An example of the M/q-dependence of observed velocity is found in the thermal solar wind shown in (Figure

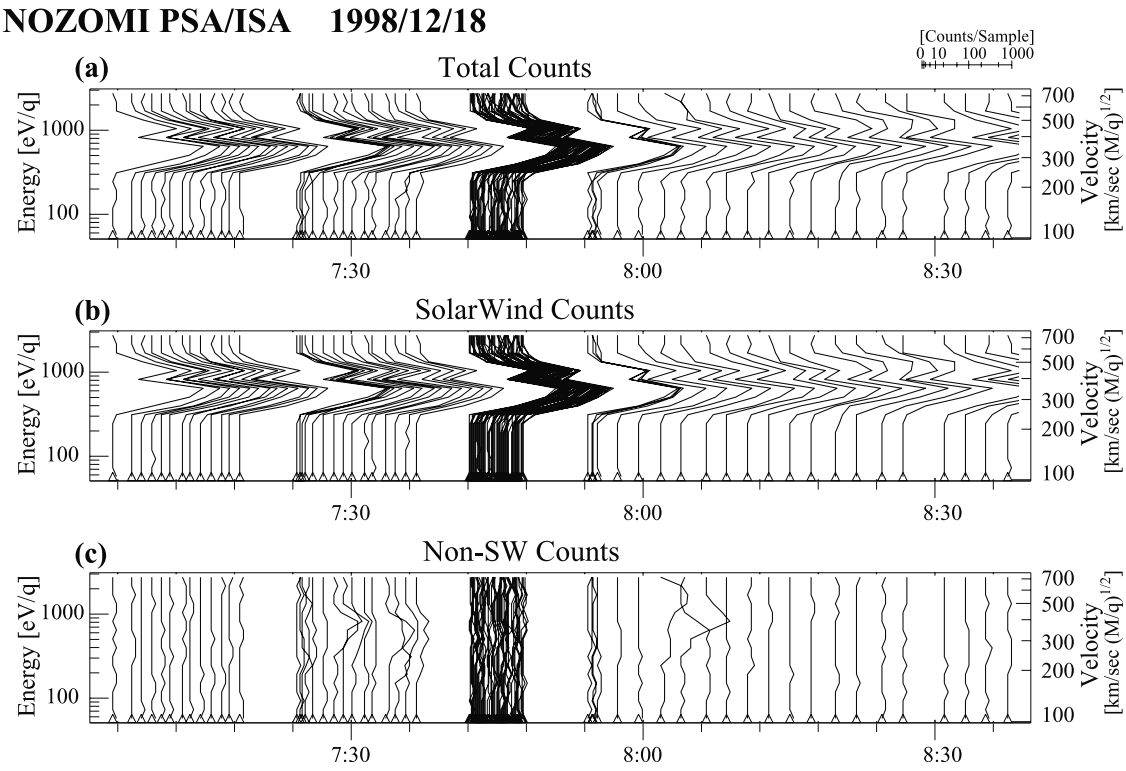

Figure 3. Time series of the counting rate observed by PSA/ISA on board Nozomi. From top to bottom, counting rate for total ions, solar wind ions, and nonthermal ions are plotted. Triangles on the time axis show the time of observation. Two notable peaks in panels (a) and (b) are the solar wind protons and the α particles. Small counts with $10 \sim 20$ around 0730 and 0800 UT are the nonthermal ions. They have almost the same energies as the solar wind protons. Nonthermal ions are clearly absent during $0740 \sim 0800$ UT.

3b). Solar wind is mainly composed of protons ($M = 1$ and $q = 1$) and α particles ($M = 4$ and $q = 2$). The PSA/ISA observation can divide them under the condition that they have the same real velocity in the solar wind. Two peaks of the count rate appear at the observed velocity of ~350 km/sec and ~500 km/sec. The ratio of their observed velocity is $\sqrt{2}$. We interpreted that both the protons and the α particles have a real velocity $v_{real} \sim 350$ km/sec but the α particles have been observed as if they had a velocity of $v_{real} = \sqrt{M/q} \times v_{obs} \sim \sqrt{2} \times 350 \sim 500\mathrm{km/sec}$.

[32] We can estimate the mass to charge ratio of the nonthermal ions by their trajectory in the $V_E - V_C$ space. A particle motion in a uniform solar wind is formulated by a simple theory and can be treated as a sum of drift motion and gyration. The drift motion is called $E \times B$-drift and is independent of mass and charge of ions. When many particles have various gyrophases, they form a ring in the $V_E - V_C$ space due to the gyration, of which the center is the $E \times B$-drift velocity $(V_E, V_C) = (0, V_{SW\perp})$, where $V_{SW\perp}$ is a solar wind velocity perpendicular to the magnetic field.

[33] Since the observational data by PSA/ISA contain the information on M/q, the observed velocity is $\sqrt{M/q}$ times larger than the real velocity from equation (2). If the observed ions have a different mass or charge from the protons, their $E \times B$-drift velocity should be $\sqrt{M/q}V_{SW,\perp}$ according to the PSA/ISA as illustrated in Figure 6.

[34] In Figure 7, the estimated values of the $E \times B$-drift velocities for different numbers of M/q are shown in the phase space plot of nonthermal ions, which is identical to (Figure 5a). Solar wind velocities perpendicular to the magnetic field were 139.9 km/sec at 0734 UT and 245.0 km/sec at 0801 UT. Determining the center of the ring is difficult because the data deviate strongly at 0734 UT. The center of the ring seems to locate on the V_C-axis with $M/q < 1$. However, we concluded that the M/q is unity and the species of the nonthermal ions is a proton. The value of M/q is unity because M/q cannot be smaller than 1. We can conclude the species of the nonthermal ions is a proton.

4.2. Model Calculation of the Nonthermal Ions

[35] Assuming that the nonthermal ions are protons, we traced the trajectories of test particles back in time following the equation of motion as shown below to estimate the source location:

$$\frac{d^2x}{dt^2} = \frac{e}{m_p}\left(E + \frac{dx}{dt} \times B\right), \tag{3}$$

where e and m_p is the proton charge and mass, E is the electric field, and B is the magnetic field. The calculation started from the satellite location with the velocity observed by PSA/ISA. We assumed a uniform magnetic field of $|B| = 3$ nT and a constant solar wind velocity of $V_{SW} = 350$ km/sec, which are the averaged values during the observation.

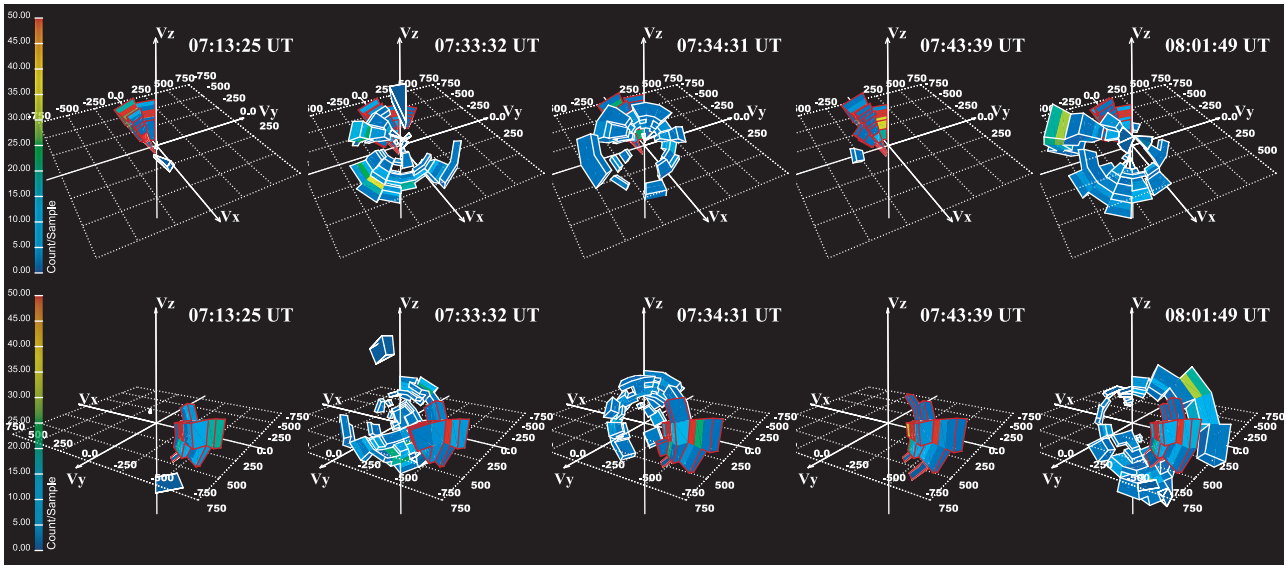

Figure 4. Time series of the 3-D velocity distribution in the GSE coordinate system. The upper and lower panels show velocity distributions seen from different angles. The ions with red and white frames are nominal solar wind and nonthermal ions, respectively. The two component can easily be distinguished because the solar wind components are very compact and have clear bound in the velocity space.

The magnetic field orientation was estimated from the anisotropy of the electrons, as explained. Further, the convection electric field ($E = -V_{SW} \times B$) was assumed in the calculation.

[36] (Figure 8a) shows the result of calculation, which indicates that most of the ions come from the dayside of the Moon. This implies that the nonthermal ions are generated at or around the dayside of the Moon. The dayside region was the magnetized region of the Moon on that day. Some of the ions look like they do not come from the Moon, but their trajectories pass the lunar surface very closely. The IMF parameters have ambiguities in an amplitude of about 1 nT and in a direction of about 20°, and the plasma waves in the solar wind or in the lunar forewake, such as those observed by *Farrell et al.* [1996], may scatter the ion trajectories.

4.3. Initial Velocities of Nonsolar Wind Ions

[37] Knowing the initial velocities of the lunar related ions is vital to specifying the generation mechanism. For example, if the nonthermal ions have zero initial velocity, they might be pickup ions originating from the lunar exosphere because neutral hydrogens in the exosphere have very small thermal velocities.

[38] (Figure 8b) shows the initial velocities of the lunar ions when they are released into interplanetary space. The initial velocities are derived from the model calculation explained in the previous section. The result shows the initial velocities of the lunar ions are close to or larger than those of the solar wind protons. We checked several factors to confirm this conclusion.

[39] First, we checked the ambiguity of the IMF parameters used in our model calculation. We confirmed that the initial velocities had not changed very much after additional model calculations with different but possible magnetic field strengths and directions. We found that the initial velocities should be several hundred km/sec.

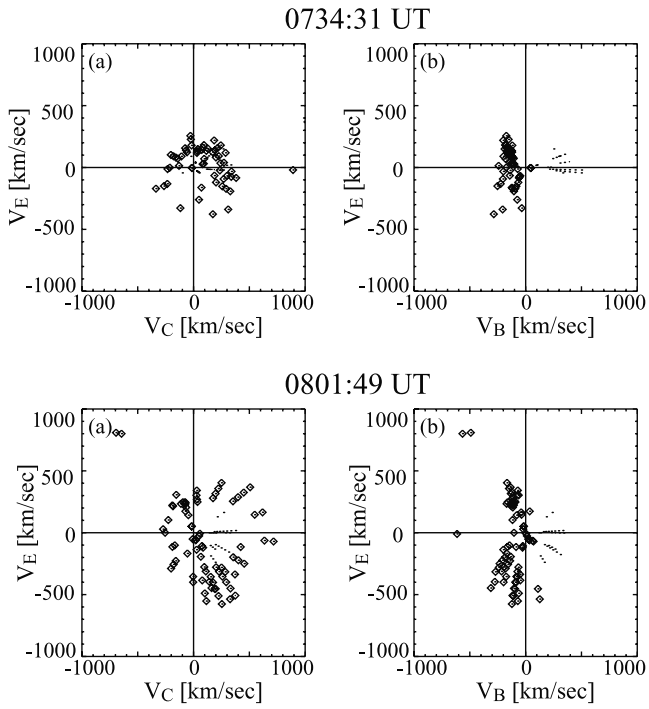

Figure 5. Velocity distribution of nonthermal ions observed by the PSA/ISA projected into the plane perpendicular to (a) the magnetic field direction and (b) the convection electric field direction. V_B, V_E, and V_C represent the apparent velocity parallel to the direction of the magnetic field, the convection electric field, and the $E \times B$-drift, respectively. Diamond symbols are the observed velocity of the nonthermal ions and dotted symbols are the observed velocity of the solar wind. Partial ring structures of nonthermal ions are seen in (a).

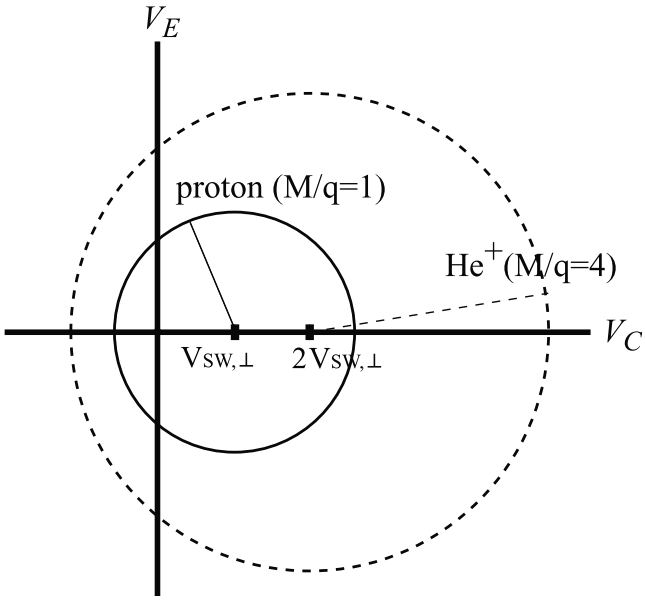

Figure 6. Expecting trajectory of nonthermal ion in the perpendicular velocity phase space. The solid circle shows the proton trajectory in the velocity space and the broken line shows the He^+ trajectory. The circle of the trajectory of particles other than protons is $\sqrt{M/q}$ times larger. Estimating the M/q state is possible by obtaining the center of the ring from the observed ion distribution.

[40] Second, we checked the scattering of the ions in the solar wind before they were observed by the spacecraft. Because the magnetometer could not detect waves correctly during the observation, the possibility cannot be ruled out observationally. However, the process does not seem feasible. The nonthermal ions only experienced one or two gyro rotations, which is not enough to be scattered. They most likely have large initial velocities.

[41] We also point out that the parallel velocities of the lunar ions in (Figure 5b) are several hundred km/sec, which is of the same order as or larger than the solar wind velocity. The parallel velocity is opposite to the solar wind parallel velocity. A simple theory that accounts for the ring structure is the collective $E \times B$-drift. This mechanism only regulates the phenomenon in the plane perpendicular to the magnetic field. The parallel velocity is conserved because no forces parallel to the magnetic field act on the ions.

[42] From those facts, we conclude that the magnitude of the initial velocities should be almost the same as, or larger than, that of the solar wind protons. A large initial velocity is an important clue to discuss the generation mechanism of the nonthermal ions near the Moon as proven in section 4.5.

4.4. Relationship With the Magnetic Field Direction

[43] Nonthermal ions were detected during the Nozomi lunar swing-by but they disappeared once between 0740 and 0800 UT (see Figures 1 and 3). One explanation of the disappearance is that the generation of nonthermal ions ceased during this interval. Another idea is that the external electromagnetic conditions changed during the interval. Discussing the first idea is impossible due to the lack of data. We examine the second idea in this section.

[44] Based on the idea of $E \times B$-drift, a particle with no initial velocity moves in a plane determined by V_{SW} and B. Small initial thermal velocities parallel to the magnetic field line only cause the particle orbits to slightly deviate from that plane. This means that the nonthermal ions can be only observed under the condition that both the an observer and the source location are in or near the plane determined by V_{SW} and B.

[45] We used a large number of protons for the test particle calculations to verify this idea When a velocity vector of a test particle at the satellite location is given, the particle can be traced back in time and we can determine whether the particle trajectory has been connected to the lunar dayside or not. A test particle whose trajectory is connected to the lunar dayside could potentially be a lunar related ions. We used 4096 test particles with velocity vectors corresponding to 4096 bins into which the PSA/ISA can divide the velocity space (32 for energy step, 16 for azimuth, and 8 for elevation). A number of ions whose trajectory is connected to the lunar dayside will be obtained among 4096 test particles under given magnetic and electric field conditions. This number is a good parameter for the observation conditions of lunar related ions. We assumed a uniform 3-nT magnetic field, a uniform 350 km/sec solar wind velocity, and a resulting uniform convection electric field. The direction of the magnetic field was varied azimuthally and elevationally within ±20° around the inferred value to consider the estimation error.

[46] Figure 9 shows the result of our calculations. The numbers of test particles whose trajectory was connected to the lunar dayside obtained for 0734, 0743, and 0801 UT are shown as a function of the azimuthal and the elevational angles of the magnetic field. It turned out that the nonthermal ions of lunar origin can be observed under the given condition of the solar wind magnetic field at 0734 and 0801 UT, but they cannot be observed at 0743 UT even if the 20° estimation error of the magnetic field orientation is considered.

[47] The result of our test particle calculation is consistent with our expectation, and we conclude that the nonthermal ions disappear because of the orientation change of the solar wind magnetic field.

4.5. Generation Mechanism of Nonthermal Ions

[48] In this section we discuss possible generation mechanisms of nonthermal ions near the Moon in the following order: 1) solar wind protons deflected by IMF disturbances,

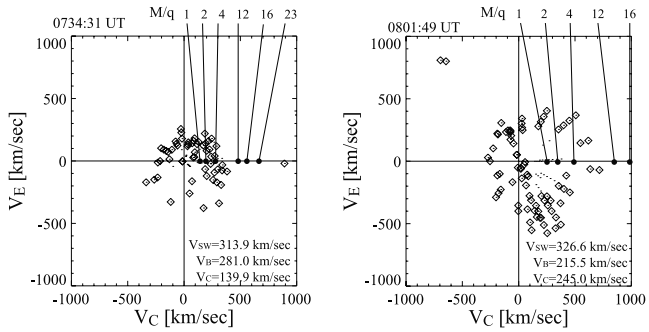

Figure 7. Velocity distribution of nonthermal ions observed by the PSA/ISA as in (Figure 5a). Drift velocities for different values of $\sqrt{M/q}$ of nonthermal ions are shown.

independent of the Moon; 2) protons reflected by the Earth's bow shock; 3) heavy ions, which are photoionized or sputtered by the solar wind or by micrometeorites, escaped from the surface of the Moon; 4) protons or heavy ions ionized by photoionization, charge exchange; or energetic electron impact in the lunar exosphere; or 5) solar wind protons deflected in the vicinity of the Moon.

[49] The first mechanism can be readily ruled out because the nonthermal ions only emerged when the satellite was very close to the Moon, and the result of the model calculation (Figure 8) tells us that the source is the Moon.

[50] The second mechanism can be ruled out even if this mechanism seems to be the most plausible at first glance. Some protons injected into the Earth's shock is reflected by the shock potential at the front, and are reflected back to the upstream region [*Thomsen*, 1985]. When they reach the Nozomi, they must have a ring structure in the velocity phase space. However, this mechanism is not realized because the model calculation shows that the source regions are not the Earth even if the 20° error of the magnetic field estimation is considered.

[51] The third mechanism is based on the idea that lunar material is ejected out to the interplanetary space. *Hilchenbach et al.* [1991] and *Mall et al.* [1998] observed such a component in the downstream of the Moon. However, this mechanism can also be ruled out because the observed M/q is too small in our case.

[52] The fourth mechanism is an analogy of the pickup ions near comets, Venus, and Mars. Our analysis of the M/q state shows that the species of nonthermal ions is proton. When neutral hydrogens are ionized in the dayside of the Moon, the initial velocities of the generated protons must be very small. This contradicts our observations. One may say that the small magnetized regions on the surface of the Moon create perturbation in the solar wind and generate electromagnetic waves that accelerate the ionized protons at a low altitude. If this is the case, very thin layer near the Moon must have an effective acceleration mechanism. This also does not seem feasible.

[53] The fifth mechanism is the most plausible mechanism for interpreting our observation, because it can explain the M/q state and the large initial velocity of the ions. The Moon has neither a global magnetosphere nor bow shock. This means that global-scale electromagnetic disturbances cannot be created around the Moon and, consequently, they cannot act as an ion deflector. One possible candidate for the deflector is the floating potential of the Moon body embedded in the solar wind. Another candidate are the small-scale magnetic field anomalies distributed on the surface of the Moon or some mechanisms related to the anomalies. We further discuss this mechanism in the next section.

4.6. Proton Deflector in the Vicinity of the Moon

[54] When the solar wind ions are deflected preserving the first adiabatic invariant such as formed in the mirror reflection, the reflected ions have a two-stream beam structure in the velocity space. The beam instability increases the occupancy of the reflected ions in the velocity

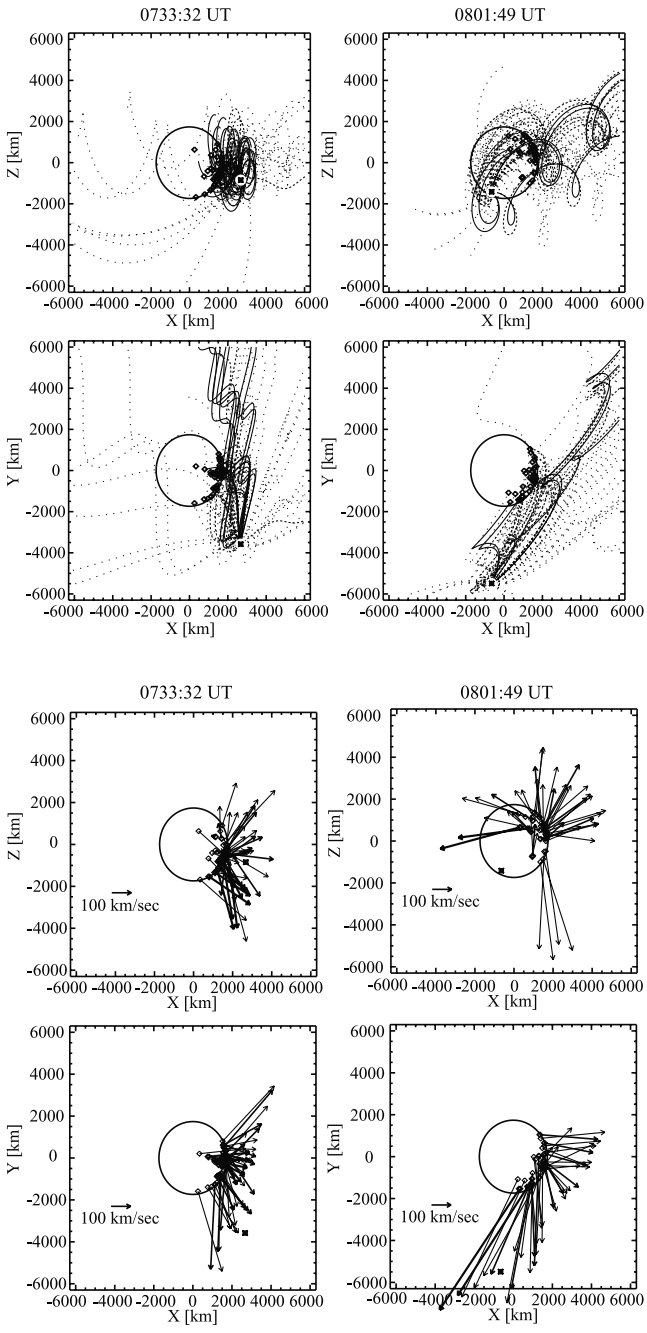

Figure 8. (opposite) Results of model calculation following the equation of motion for observed nonthermal ions at 0733:32 and 0801:49 UT. Circles at the center of each figure represent the Moon which is illustrated to scale. We used LCGSE coordinate system. The satellite position is shown by black symbols in each panel ((X, Y, Z) = (2670 [km], −3580, 690) at 0733 UT and (X, Y, Z) = (−650, −5480, −1420) at 0801 UT). (a) Model calculated trajectory of the incoming protons toward Nozomi. Solid and dotted lines are the ion trajectories. Trajectories indicated by solid lines have larger counting rates than those indicated by dotted lines. The diamond marks on the lunar surface show the foot location of the nonthermal ions. Most of the ions come from the dayside of the Moon. (b) Generated locations and initial velocities of the lunar ions at the surface of the Moon. Lunar ions have a large initial velocity comparable to, or larger than, the solar wind protons.

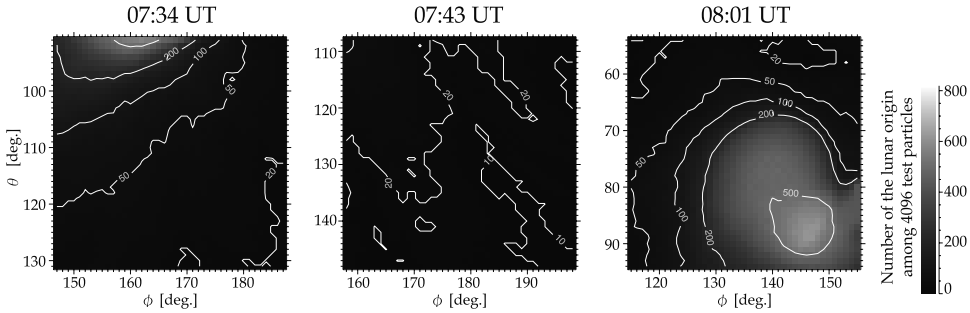

Figure 9. Mapping of numbers of the particles that have trajectories that are connected to the lunar surface, out of 4096 test particles, at 0734, 0743, and 0801 UT. The horizontal and vertical axes are azimuthal (ϕ) and elevational (θ) angles of the magnetic field. The center of the panel corresponds to the estimated direction of the magnetic field. Ions from the lunar surface can be observed by Nozomi under a given solar wind magnetic field condition at 0734 and 0801 UT, but they cannot be observed at 0743 UT.

space and the reflected ions form a shell-like structure. This mechanism cannot explain our observation of the partial ring structure. The deflection mechanism near the Moon must destroy the first adiabatic invariant so that some dynamic structure must exist in the vicinity of the Moon.

[55] Electrostatic potential, which is produced by the photoelectron layer on the lunar surface, could be one of the candidates. However, it is reported that the potential has been reported to reach approximately 10 volts at most [*Benson et al.*, 1975], so it cannot deflect the solar wind protons with energies of about 1 keV.

[56] Another possibility is a nonuniform magnetic field structure near the Moon surface. The Moon has some anomalous magnetic fields with horizontal scales of 100 $\sim$ 1000 km, which is comparable to, or larger than, the solar wind proton gyro radius ($\sim$80 km during the observation).

[57] Stochastic deflection due to the finite Larmor radius effect around the magnetic anomaly can be considered, but explaining the observed protons with a larger initial velocity than that of the solar wind.

[58] The miniature bow shock around the anomalous magnetic field proposed by *Lin et al.* [1998] and *Harnett and Winglee* [2000] is also another possible candidate and it is the most suitable for interpreting the observation. It can explain the protons with a large initial velocity in the upstream region of the collisionless shock [e.g., *Paschmann et al.*, 1981; *Thomsen*, 1985]. Large magnetic anomalies on 1000-km scales are distributed on the farside of the Moon so that the interaction between the anomaly and the solar wind is the most effective during the observation when the moon phase is new moon.

[59] We suggest that deflection mechanism of the miniature bow shock is due to the interaction between the lunar crustal magnetic anomalies and the solar wind, but Nozomi's observation is very limited in space and time, so the problem of the proton deflection mechanism remains unsolved. To understand the deflection mechanism, we should observe the height profile of the 3-D velocity distribution functions and the spatial distribution of the nonthermal ions.

5. Summary

[60] Having analyzed the 3-D distribution functions of ions obtained in the vicinity of the Moon, we found that protons are injected into the interplanetary space from the Moon with fluxes of $10^6 \sim 10^7/cm^2$ sec. Their source is the dayside region of the Moon, where the magnetic anomalies was mainly distributed during the observation. They are observed only under the specific condition of the solar wind and the spacecraft location relative to the Moon body. They have large initial velocities comparable to, or larger than, those of the solar wind and have the velocity distribution function of a partial ring structure.

[61] Based on these results and our discussion, we propose the following scenario for lunar ions: the vicinity of the Moon must have a deflector which deflect a part of the solar wind protons around the lunar surface while most protons are absorbed when they reach the lunar surface. The miniature bow shock, resulting from the interaction between the lunar magnetic anomalies and the solar wind, is the most likely candidate. Note that the first adiabatic invariant is broken during the deflection. The deflected protons have large velocities due to the bulk velocity of the solar wind, and they move under the force exerted by the convection electric field and gyrate around the magnetic field in the solar wind. This motion forms a partial ring structure with large initial velocities in the velocity phase space as observed by the PSA/ISA. The observation of nonthermal ions proves that a dynamic electromagnetic structure exists in front of the Moon.

[62] Lunar ions are important for studying the plasma environment near the Moon. But the data was not sufficient to comprehensively understand the physics of the lunar ions, especially the deflection mechanism of the solar wind. We will continue model calculations to investigate the deflection mechanism and estimate the deviation of the trajectory of the lunar ions. We also suggest global in situ observations of the 3-D velocity distribution functions to study the acceleration mechanism. In addition, we suggest observing the lunar ions from a distance of several lunar radii in various electromagnetic environments, various $F_{10.7}$ parameters, moon phases, or for different amounts of micrometeorites. These observations will enable us to completely understand the generation mechanisms and the diffusion processes of lunar ions. Understanding these mechanisms also enhances our knowledge on pickup ions around unmagnetized bodies, like comets, Mars, and Venus.

[63] **Acknowledgments.** We appreciate the assistance of ACE Science Center at Caltech for allowing us to use the solar wind data from the ACE spacecraft. We would like to thank D. J. McComas at LANL and SWEPAM team for plasma data and N. F. Ness at BRI and MAG team for magnetic field data. We also thank T. Mukai and T. Terewawa for valuable suggestions and comments. One of the authors (Y. Futaana) was supported by a grant of the Research Fellowship of the Japan Society for the Promotion of Science for Young Scientists.

[64] Lou-Chang Lee and Chin S. Lin thank two reviewers for their assistance in evaluating this paper.

References

Asbridge, J. R., S. J. Bame, and I. B. Strong, Outward flow of protons from the earth's bow shock, *J. Geophys. Res.*, *73*, 5777–5782, 1968.

Benson, J., J. W. Freeman, and H. K. Hills, The lunar terminator ionosphere, *Proc. Lunar Sci. Conf., VIth*, 3013–3021, 1975.

Cladis, J. B., W. E. Francis, and R. R. Vondrak, Transport toward earth of ions sputtered from the moon's surface by the solar wind, *J. Geophys. Res.*, *99*, 53–64, 1994.

Colburn, D. S., R. G. Currie, J. D. Mihalov, and C. P. Sonett, Diamagnetic solar-wind cavity discovered behind the moon, *Science*, *158*, 1040–1042, 1967.

Dolginov, S. S., Y. G. Yeroshenko, L. N. Zhuzgov, and N. V. Pushkov, Investigations of the magnetic field of the moon, *Geomagn. Aeron.*, *1*, 18–25, 1961.

Dyal, P., C. W. Parkin, and W. D. Daily, Magnetism and the interior of the Moon, *Rev. Geophys. Space Phys.*, *12*, 568–591, 1974.

Farrell, W. M., R. J. Fitzenreiter, C. J. Owen, J. B. Byrnes, R. P. Lepping, K. W. Ogilvie, and F. Neubauer, Upstream ULF waves and energetic electrons associated with the lunar wake: Detection of precursor activity, *Geophys. Res. Lett.*, *23*, 1271–1274, 1996.

Feldman, W. C., J. R. Asbridge, S. J. Bame, M. D. Montgomery, and S. P. Gary, Solar wind electrons, *J. Geophys. Res.*, *80*, 4181–4196, 1975.

Futaana, Y., S. Machida, Y. Saito, A. Matsuoka, and H. Hayakawa, Counterstreaming electrons in the near vicinity of the Moon observed by plasma instruments on board NOZOMI, *J. Geophys. Res.*, *106*, 18,729–18,740, 2001.

Harnett, E. M., and R. Winglee, Two-dimensional MHD simulation of the solar wind interaction with magnetic field anomalies on the surface of the Moon, *J. Geophys. Res.*, *105*, 24,997–25,007, 2000.

Hilchenbach, M., D. Hovestadt, B. Klecker, and E. Möbius, Detection of singly ionized energetic lunar pick-up ions upstream of Earth's bow shock, in *Proceedings of Solar Wind Seven*, edited by E. Marsch and G. Schwenn, pp. 349–355, Pergamon, New York, 1991.

Hilchenbach, M., D. Hovestadt, B. Klecker, and E. Möbius, Observation of energetic lunar pick-up ions near earth, *Adv. Space Res.*, *13*, 10,321–10,324, 1993.

Hood, L. L., and C. R. Williams, The lunar swirls: Distribution and possible origins, *Proc. Lunar Sci. Conf., XIXth*, 99–113, 1989.

Hood, L. L., A. Zakharian, J. Halekas, D. L. Mitchell, R. P. Lin, M. H. Acuña, and A. B. Binder, Initial mapping and interpretaion of lunar crustal magnetic anomalies using Lunar Prospector magnetometer data, *J. Geophys. Res.*, *106*, 27,825–27,839, 2001.

Lin, R. P., K. A. Anderson, and L. L. Hood, Lunar surface magnetic field concentrations antipodal to young large impact basins, *Icarus*, *74*, 529–541, 1988.

Lin, R. P., D. L. Mitchell, D. W. Curtis, K. A. Anderson, C. W. Carlson, J. McFadden, M. H. Acuña, L. L. Hood, and A. Binder, Lunar surface magnetic fields and their interaction with the solar wind: Results from Lunar Prospector, *Science*, *281*, 1480–1484, 1998.

Lundin, R., A. Zakharov, R. Pellinen, H. Borg, B. Hultqvist, N. Pissarenko, E. M. Dubinin, S. W. Barabash, I. Liede, and H. Koskinen, First measurements of the ionospheric plasma escape from Mars, *Nature*, *341*, 609–612, 1989.

Lyon, E. F., H. S. Bridge, and J. H. Binsack, Explorer 35 plasma measurements in the vicinity of the Moon, *J. Geophys. Res.*, *72*, 6113–6117, 1967.

Machida, S., Y. Saito, Y. Ito, and H. Hayakawa, Instrumental characteristics of the Electron Spectrum Analyzer (ESA) onboard the Planet-B mission and observational perspectives of the electron measurements, *Earth Planets Space*, *50*, 207–211, 1998.

Mall, U., E. Kirsch, K. Cierpka, B. Wilken, A. Söding, F. Neubauer, G. Gloeckler, and A. Galvin, Direct observation of lunar pick-up ions near the Moon, *Geophys. Res. Lett.*, *25*, 3799–3802, 1998.

Montgomery, M. D., S. J. Bame, and A. J. Hundhausen, Solar wind electrons: Vela 4 measurements, *J. Geophys. Res.*, *73*, 4999–5003, 1968.

Mukai, T., W. Miyake, T. Terasawa, M. Kitayama, and K. Hirao, Plasma observation by Suisei of solar-wind interaction with comet Halley, *Nature*, *321*, 299–303, 1986.

Ness, N. F., K. W. Behannon, C. S. Scearce, and S. C. Cantarano, Early results from the magnetic field experiment on Lunar Explorer 35, *J. Geophys. Res.*, *72*, 5769–5778, 1967.

Ogilvie, K. W., J. D. Scudder, and M. Sugiura, Electron energy flux in the solar wind, *J. Geophys. Res.*, *76*, 8165–8173, 1971.

Paschmann, G., N. Sckopke, I. Papamastorakis, J. R. Asbridge, S. J. Bame, and J. T. Gosling, Characteristics of reflected and diffuse ions upstream from the Earth's bow shock, *J. Geophys. Res.*, *86*, 4355–4364, 1981.

Peredo, M., J. A. Slavin, E. Mazur, and S. A. Curtis, Three-dimensional position and shape of the bow shock and their variation with Alfvénic, sonic and magnetosonic Mach numbers and interplanetary magnetic field orientation, *J. Geophys. Res.*, *100*, 7907–7916, 1995.

Russell, C. T., and B. R. Lichtenstein, On the source of lunar limb compressions, *J. Geophys. Res.*, *80*, 4700–4711, 1975.

Schubert, G., and B. R. Lichtenstein, Observations of Moon-plasma interactions by orbital and surface experiments, *Rev. Geophys.*, *12*, 592–626, 1974.

Terasawa, T., T. Mukai, W. Miyake, M. Kitayama, and K. Hirao, Detection of cometary pickup ions up to 10^7 km from comet Halley: Suisei observation, *Geophys. Res. Lett.*, *13*, 837–840, 1986.

Thomsen, M. F., Upstream suprathermal ions, in *Collisionless Shocks in the Heliosphere: Reviews of Current Research, Geophys. Monogr. Ser.*, vol. 35, edited by B. T. Tsurutani and R. G. Stone, pp. 253–270, AGU, Washington, D. C., 1985.

Yamamoto, T., and K. Tsuruda, The PLANET-B mission, *Earth Planets Space*, *50*, 175–181, 1998.

Y. Futaana and S. Machida, Department of Geophysics, Graduate School of Science, Kyoto University, Kyoto, 606-8502, Japan. (futaana@kugi.kyoto-u.ac.jp)

H. Hayakawa, A. Matsuoka, and Y. Saito, Institute of Space and Astronautical Science, 3-1-1 Yoshinodai, Sagamihara, Kanagawa 229-8510, Japan.